

Relativistic Effects on Galaxy Redshift Samples due to Target Selection

Shadab Alam^{1,2,3} ^{*}, Rupert A. C. Croft^{1,2}, Shirley Ho^{1,2,4,5}, Hongyu Zhu^{1,2}
and Elena Giusarma^{1,2,4,5}

¹ Department of Physics, Carnegie Mellon University, 5000 Forbes Ave., Pittsburgh, PA 15213

² McWilliams Center for Cosmology, Carnegie Mellon University, 5000 Forbes Ave., Pittsburgh, PA 15213

³ Institute for Astronomy, University of Edinburgh, Royal Observatory, Blackford Hill, Edinburgh, EH9 3HJ, UK

⁴ Lawrence Berkeley National Laboratory (LBNL), Physics Division, Berkeley, CA 94720-8153, USA

⁵ Departments of Physics and Astronomy, University of California, Berkeley, CA 94720, USA

25 September 2017

ABSTRACT

In a galaxy redshift survey the objects to be targeted for spectra are selected from a photometrically observed sample. The observed magnitudes and colours of galaxies in this parent sample will be affected by their peculiar velocities, through relativistic Doppler and relativistic beaming effects. In this paper we compute the resulting expected changes in galaxy photometry. The magnitudes of the relativistic effects are a function of redshift, stellar mass, galaxy velocity and velocity direction. We focus on the CMASS sample from the Sloan Digital Sky Survey (SDSS), Baryon Oscillation Spectroscopic Survey (BOSS), which is selected on the basis of colour and magnitude. We find that 0.10% of the sample (~ 585 galaxies) has been scattered into the targeted region of colour-magnitude space by relativistic effects, and conversely 0.09% of the sample (~ 532 galaxies) has been scattered out. Observational consequences of these effects include an asymmetry in clustering statistics, which we explore in a companion paper. Here we compute a set of weights which can be used to remove the effect of modulations introduced into the density field inferred from a galaxy sample. We conclude by investigating the possible effects of these relativistic modulation on large scale clustering of the galaxy sample.

Key words: gravitation; modified gravity; galaxies: statistics; cosmological parameters; large-scale structure of Universe

1 INTRODUCTION

General Relativity (GR; Einstein 1916) combined with the standard cosmological model (Λ CDM) provides the most successful theory of our universe with the minimum of external assumptions. The Λ CDM model paints a simple picture of structure formation arising from density fluctuations growing under gravity (Comer et al. 1994). For most of the Universe’s history, these perturbations obey linear perturbation theory (Mukhanov et al. 1992; Liddle & Lyth 1993; Durrer 1994; Ma & Bertschinger 1994; Bruni & Lyth 1994; Kopeikin et al. 2001; Bernardeau et al. 2002; Lagos et al. 2016). The density field predicted by these theories have very specific statistical properties with multiple unique features (Peebles & Yu 1970; Eisenstein et al. 2005; Bassett & Hlozek 2010; Coil 2013). We can measure most of the physical quantities of the universe just by comparing one, two, three and higher point statistics of the pre-

dicted matter density field. Galaxies provide us with a window on the underlying matter density field of the universe. In the limit of linear perturbations, galaxies can be assumed to form at the high-density peaks of the underlying matter density field and should have same clustering properties up to a multiplicative constant (galaxy bias) (Bardeen et al. 1986; Cole & Kaiser 1989). Therefore creating three-dimensional maps of galaxies and studying their clustering properties provides one of the most precise ways to measure physical properties of our universe. In this paper, we address one of the complications of making these maps from galaxy redshift surveys which is usually ignored: the effect of peculiar velocities on galaxy photometry and thus the target selection.

Carrying out large galaxy surveys has been a challenging task, which was made easier by the development of CCD cameras (Beletic & Amico 1998). Many astronomy projects were involved in the development and adoption of CCD technology for telescopes (Arnaud et al. 1994; Abe et al. 1997; Bauer & de Kat 1998; Boulade 1998; Fukugita et al. 1996; Gunn et al. 1998). These have led to various photometric surveys covering increasingly large

* Email: salam@roe.ac.uk

<https://sites.google.com/site/salamcosmology>

parts of sky with improved depth and resolution (York et al. 2000; Gladders & Yee 2005; Kaiser et al. 2010; Takada 2010; Gilbank et al. 2011, DES¹). Such surveys provide an excellent map of the angular distribution of galaxies, but precise measurements of the cosmological line-of-sight distance, and hence creation of three dimensional maps, requires redshifts (z). The redshift quantifies the wavelength shift of features in galaxy spectra and hence requires observing galaxy's spectral energy distributions (SED). The measurement of galaxy SED requires targeting each galaxy individually and is a very expensive process. An early large galaxy redshift surveys was the CfA redshift survey (Geller & Huchra 1989) which observed 22000 galaxies one at a time. Galaxy surveys targeting much large numbers of galaxies for SED measurement became possible with the advent of optical fibres combined with the ability to observe hundreds of SEDs in a single exposure. The huge increase in the number of spectra that we could observe started the era of large galaxy redshift surveys e.g: Shectman et al. (1996, LCRS), Colless et al. (2003, 2dF), Jones et al. (2009, 6dF), Eisenstein et al. (2011, SDSS-III), Blake et al. (2011, WiggleZ), Newman et al. (2013, DEEP2), Garilli et al. (2014, VIPERS), Liske et al. (2015, GAMA).

To make this process efficient, it is important to have prior knowledge about the location of possible targets. Therefore, generally galaxy redshift surveys require samples of objects observed photometrically to serve as parent sample. Various algorithms and knowledge of galaxy evolution models are employed to create subsamples of such parent samples to be targeted for spectra (for example Reid et al. (2016)). Generally, these selection algorithms use various magnitude and colour cuts to define these subsamples. We know that the observed magnitudes and colours of galaxies are affected by their peculiar motion (Teerikorpi 1997). This can influence the final spectroscopic galaxy target sample obtained after following the target selection rules (Kaiser 2013). Such effects will act to modulate the observed galaxy density in the observed sample, in a way which will be correlated with galaxy properties including redshift, mass and velocity. This could in principle introduce new features into the measured clustering of galaxies and also bias the physical properties inferred from such clustering observations.

In this paper, we examine the special relativistic effects that galaxy peculiar velocity have on their observed SEDs and the photometric quantities derived from them. We then discuss the impact of these effects on an observed sample of galaxies. We use the Sloan Digital Sky Survey III (SDSSIII) Baryon Oscillation Spectroscopy Survey (BOSS) CMASS sample from Data Release 12 (DR12) as an example to show how relativistic effects will impact target selection which uses cuts in the magnitude and colour plane. We then discuss how these introduce density modulation in the observed sample. We define a weighting scheme to compensate for such modulation and look at its effect on the clustering signal. We conclude with a discussion about the impact of such effects on the large scale structure analyses. We note that we restrict ourselves here to the effect of peculiar velocities on spectroscopic target selection. This is distinct from the effect of velocities on the properties of galaxies inferred from the spectroscopic sample (e.g., Kaiser & Hudson 2015; Bacon et al. 2014). We would like to stress here that the main focus of and motivation for the paper is the derivation of the relativistic weights. The impact on the clustering signal is just one of the areas which can be assessed using these weights. We are most interested however in the weights themselves, which

can be used to model the impact of relativistic effects (specifically relativistic beaming) on galaxy clustering. We investigate this aspect in our companion paper Zhu et al. (2017).

2 EFFECTS OF PECULIAR VELOCITIES ON GALAXY SPECTRA

We study the relativistic effects of galaxy motion on galaxy spectra and how they affect observed galaxy flux and colour. This will help us estimate the impact of such observational effects on our final observed samples. We consider two kinds of effects. The first is the redshift or blueshift applied to the spectrum due to relative motion between the observer and galaxy. The second is the change in flux coming from relativistic boost and beaming. Note that we do not consider the impact of magnification caused by gravitational lensing (Schmidt et al. 2012; Ménard et al. 2010).

2.1 Relativistic Doppler effect

The relativistic Doppler effect shifts the observed wavelength of a photon with respect to the emitted wavelength in a manner which depends on the line of sight velocity of the source. The observed wavelength and emitted wavelength for a galaxy moving along the line-of-sight are related by the following equation, where $\beta_{los} = v_{los}/c$ is the ratio of line of sight velocity (v_{los}) and the speed of light (c):

$$\lambda_o = \lambda_e \sqrt{\frac{1 - \beta_{los}}{1 + \beta_{los}}}. \quad (1)$$

Here λ_o and λ_e are the observed and emitted wavelengths respectively. The galaxy's velocity along the line of sight consists of two components. First component is the Hubble velocity due to the expansion of the universe (denoted by v_e) while the second component is due to local dynamics, the peculiar velocity and denoted by v_p . The total line-of-sight velocity of a galaxy v_{los} is given by relativistic addition of the two components under the assumption of negligible matter density so that

$$v_{los} = \frac{v_e + v_p}{1 + \frac{v_e v_p}{c^2}}. \quad (2)$$

The expansion of the Universe acts to redshift the galaxy spectrum, and peculiar velocities lead to additional shifts. This implies that photometric bands see different parts of the spectrum for galaxies with different redshifts. Accounting for this shift leads to the well known K-correction, (see for example the case of massive galaxies Hogg et al. 2002; Blanton et al. 2003b). In order to apply a K-correction to galaxy magnitudes in different bands, it is necessary to use an estimate of the galaxy redshift. In the present paper, we concern ourselves with target selection for galaxy spectroscopic redshift surveys, and we assume that this target selection is carried out using galaxy magnitudes before a redshift is known, and hence without K-corrections. Photometric redshifts could instead be used to compute K-corrections first, but we consider surveys such as BOSS/CMASS (Reid et al. 2016) and the SDSS main galaxy sample (Strauss et al. 2002) where this is not done.

First, we note that the effect of shift in wavelengths due to different components of the galaxy velocity can be separated as follows:

$$\left(\frac{\lambda_o}{\lambda_e}\right)^2 = \left(\frac{1 - \beta_{los}^e}{1 + \beta_{los}^e}\right) \left(\frac{1 - \beta_{los}^p}{1 + \beta_{los}^p}\right) \quad (3)$$

¹ <http://www.darkenergysurvey.org/survey/>

Equation 3 shows that the Doppler shifts in wavelength due to different velocity components is separable and hence justifies our treatment to separate peculiar velocity from the Hubble velocity due to the expansion of the Universe. We note that additional terms such as that due to the gravitational redshift/Sachs-Wolfe effect are also relevant, and are treated in our companion paper (Zhu et al. 2017). To linear order in perturbation theory, the combined effects are described in detail by e.g., Yoo (2014); Bonvin (2014). We also note that if galaxy band magnitudes were K-corrected using the observed galaxy redshift this would take into account the effect of peculiar velocities as well as the Hubble expansion and other components. As stated above, such K-corrections are not relevant for the target selection considered here.

It is important to define the sign convention for velocity to avoid any confusion. From now on we use positive velocity and β to indicate that the line-of-sight component of galaxy peculiar velocity is toward the observer. Negative velocity will imply that the galaxy's line-of-sight component of velocity is moving away from the observer. In the situation when a galaxy is moving with velocity $c\beta$ at an angle θ from the line-of-sight then the Doppler shift will have an additional term due to the transverse velocity. The observed wavelength and emitted wavelength for a galaxy moving in such a situation is given by the following equation, where $\gamma = 1/\sqrt{1-\beta^2}$

$$\lambda_o = \gamma(1 - \beta \cos(\theta))\lambda_e \quad (4)$$

2.2 Relativistic Beaming effect

Relativistic beaming modifies the apparent brightness of a galaxy due to its peculiar motion. The peculiar motion of galaxy through the Doppler shift modifies the energy of emitted photons and the number of photons emitted per unit time. The direction in which photons are emitted is also different in the observed frame compared to the galaxy's rest frame, leading to an anisotropic pattern of emission in the observer's frame. Taken together, these effects are known as relativistic beaming. The effect on the spectral brightness can be derived using special relativity. The spectral brightness (I_ν) of a galaxy is defined to be the energy observed per unit time, per unit area of the detector, per unit frequency and per unit solid angle²:

$$I_\nu = \frac{\Gamma E}{\sigma \Omega}, \quad (5)$$

where Γ is the number of photons emitted per unit time, E is the energy of emitted photons, Ω is the solid angle subtended by the observed galaxy and σ is the area of the detector. Each of the quantities appearing in equation 5 will be modified by the peculiar motion of the galaxy in the observed frame. The spectral brightness in the observed (telescope) frame (I_ν^o) and emitted (galaxy rest) frame (I_ν^e) are related by following equation:

$$\frac{I_\nu^o}{I_\nu^e} = \left(\frac{\nu_o}{\nu_e}\right)^3 = [\gamma(1 - \beta \cos(\theta))]^{-3}. \quad (6)$$

Here the Lorentz factor $\gamma = \frac{1}{\sqrt{1-\beta^2}}$ and θ is the angle the velocity vector makes with the line of sight direction. The above ex-

pression is derived using the fact that phase space volume is invariant under Lorentz transformations. It is proportional to the number of photon in a quantum state. This makes the quantity $\frac{I_\nu}{\nu^3}$ Lorentz invariant and leads to equation³ 6. This equation is in terms of flux per unit frequency whereas our measurements will be in flux per unit wavelength. The spectral brightness per unit frequency (I_ν) can be converted to the spectral brightness per unit wavelength (I_λ) using:

$$I_\lambda = \frac{dF}{d\lambda} = \frac{dF}{d\nu} \frac{d\nu}{d\lambda} = \frac{I_\nu}{\lambda^2} \quad (7)$$

Where we have used $\nu\lambda = c$.

Finally, the observed and emitted spectral brightness per unit wavelength can be obtained by combining equations 4, 6 and 7:

$$\frac{I_\lambda^o}{I_\lambda^e} = [\gamma(1 - \beta \cos(\theta))]^{-5} \quad (8)$$

It is important to note that relativistic beaming depends on both the magnitude and direction of the source velocity and not just its the line-of-sight component.

2.3 Effects of velocity on the observed spectra

The spectra observed for a galaxy redshift survey experience both the effects discussed in the previous two subsections: the shift in wavelength due to Doppler shift and the change in flux due to relativistic beaming.

To compute these effects on the broad band magnitudes used for target selection we can make use of some template galaxy spectra and redshift them. The spectra observed from the BOSS/CMASS survey can fulfill this purpose. We therefore now describe how the BOSS/CMASS fibre spectra are affected by peculiar velocities.

The following equation describes how the observed flux per unit wavelength (f_λ^o) is related to the emitted flux per unit wavelength (f_λ^e) at wavelength (λ_e), as a function of observed wavelength (λ_o)

$$f_\lambda^o(\lambda_o, \beta, \theta) = f_\lambda^e(\lambda_e) [\gamma(1 - \beta \cos(\theta))]^{-5} \quad (9)$$

Here the galaxy is moving with peculiar velocity $v = \beta c$ along the direction at angle θ from the line-of-sight. The observed (λ_o) and emitted (λ_e) wavelengths are related by equation 4. While deriving equation 9, we have assumed isotropic emission of light from galaxies. In the case of realistic galaxies the different components of galaxies can have a non-isotropic emission pattern. In such cases the shape of the galaxy can be aligned with tidal forces acting on it (causing so-called intrinsic alignments) and hence may show a correlation with the peculiar velocity. Modelling the anisotropic emission from galaxies and its correlation with peculiar velocity is beyond the scope of this paper but could be studied in future work.

Figure 1 shows the effect of relativistic beaming and relativistic doppler shift on the observed galaxy spectra and colour. The top panel focuses on the galaxy SED. The x-axis shows the wavelength in Å and the y-axis shows the observed flux. The colour scale represents the velocity of the galaxy in the unit of speed of

² More discussion in Hogg (1997). Section 7.4 of <http://cosmo.nyu.edu/hogg/sr/sr.pdf> is most relevant

³ A detailed derivation of these equations can be found in Goodman (2013). Chapter 1 of <http://www.astro.princeton.edu/~jeremy/heap.pdf> is most relevant

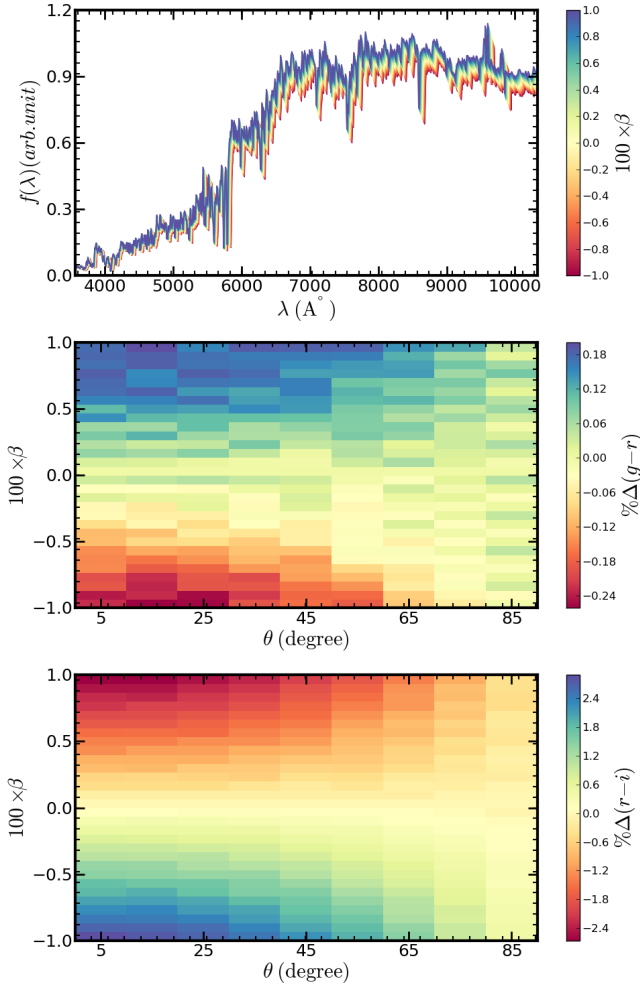


Figure 1. The relativistic effects on the spectra and observed colour of a single galaxy. The top panel shows the flux of a galaxy SEDs on the y-axis, with x-axis showing wavelength in \AA and the colour scale showing velocity. Two effects are illustrated, the first being the wavelength shift and the second being the rescaling of flux for the same wavelength as the source galaxy moves towards or away from the observer. The middle and bottom panels show the percentage change in the $g-r$ and $r-i$ colours as a function of the magnitude and direction of the galaxy velocity respectively. The change in colours are strongest when galaxy velocity is aligned towards the line-of-sight (*i.e.* $\theta = 0$), and vanishes when the galaxy velocity becomes perpendicular to the line-of-sight (*i.e.* $\theta = 90$).

light. The spectrum corresponding to $\beta = 0$ represents the emitted galaxy spectrum. We can clearly see the two effects discussed in the previous two sections. The relativistic Doppler shift causes the atomic lines to shift in wavelength. Relativistic beaming increases the observed flux for positive β (moving towards the observer) and decreases it for negative β (moving away from the observer). The middle and bottom panels show the percentage change in the $g-r$ and $r-i$ colour as a function of different velocity magnitude (varying along the y-axis) and velocity direction with respect to the line-of-sight (x-axis). The percentage change in $g-r$ colour is at the level of 0.2% when the galaxy has a peculiar velocity of 3000 km s^{-1} . For realistic velocities of around 400 km s^{-1} (See section 4.5) the change is around 0.05%. For $r-i$ colour the percentage change is significantly higher, at the level of 3% for

3000 km s^{-1} galaxies and $\sim 0.5\%$ for 400 km s^{-1} . This difference between colour bands illustrates that the strength of the relativistic selection effects will depend on galaxy spectrum and hence galaxy type in a relatively complex way.

3 EFFECTS OF VELOCITIES ON SELECTED CATALOG

Most large galaxy redshift surveys feature a two-step process of photometric target selection and spectroscopic follow-up. Grism spectroscopy and other techniques for one-step generation of galaxy redshift samples have been used in the past (e.g. Schuecker 1996; Momcheva et al. 2015; Hill et al. 2008) and will play a prominent role in the future (EUCLID: Content et al. (2010), WFIRST: Spergel et al. (2013), SPHEREx: Bock & SPHEREx Science Team (2016)). Nevertheless, fibre spectrographs are also becoming larger and photometric selection of galaxy targets will be used to generate samples of tens of millions of galaxy redshifts in the next few years (DESI Collaboration et al. 2016). We therefore focus in this paper on photometric target selection.

In order to obtain a reasonable target sample one must determine the properties of each object based on photometric magnitudes. This requires detailed modeling of the SEDs of different kinds of objects. The targets of interest are then selected from a photometric sample which has predefined depth and redshift coverage. Historically target selection was the result of simple magnitude cuts. Recent redshift surveys employ more complex sample selection with various cuts in the colour-magnitude plane (Reid et al. 2016; Prakash et al. 2016). The final observed samples will also be affected by several biases due to the interplay between the sharp magnitude cut, the luminosity function and errors in the observed magnitudes. These biases are well understood and discussed in detail by e.g., Teerikorpi (1997). We are not focusing on biases of such kind, but instead we are concerned about the modulations introduced in the inferred density field due to galaxy peculiar motion, but distinct from redshift space distortions. As mentioned in Section 2, we deal exclusively with target selection where K-corrections have not been applied to galaxy broad-band magnitudes before targets are selected. If redshifts are available and those corrections are made, the effects of peculiar velocities on galaxy colours would be nullified by the K-correction.

3.1 Magnitude limited sample

A magnitude limited sample is one which has been selected only by applying a limiting magnitude cut. The effect of peculiar velocities on such a sample is relatively simple to understand. The galaxies moving towards the observer will have their magnitudes boosted and those that are intrinsically just below the threshold will move into the sample. The galaxies moving away from an observer will have their magnitudes suppressed and hence those just above the magnitude limit will move out of the sample. We can therefore construct a simple picture in which the probability of a galaxy passing the sample cut is determined by its velocity. The constant of proportionality will depend on the true magnitude of the galaxy and its spectrum and it will always be positive. This means galaxies moving towards the observer will always have a higher probability of making the sample cut compared to galaxies moving away from the observer. This is true unless one considers an exotic galaxy SED, for example, an SED in which flux decreases with wavelength fast enough, such that the gain in flux by relativistic beaming is smaller than the reduction in flux caused by relativistic Doppler effect.

3.2 colour-Magnitude cuts

Most of the current and future galaxy redshift survey have a more complicated targeting algorithm than simple magnitude cuts. In a more complicated scenario where the sample selection has several colour and magnitude cuts, the simplest expectation that galaxies moving towards the observer will have a higher probability of making into the sample does not hold true. The exact nature of cuts, details of spectra and the galaxy population can lead to the probabilities of including galaxies moving towards the observer being smaller than those moving away from the observer. Such effects depend on the redshift, halo mass and peculiar velocity (both magnitude and direction) of the observed galaxy. This can lead to extra structure in the number density of the observed target and affect the clustering measurements. This has been assumed to be unimportant for current and future surveys. We will investigate the validity of this past assumption. Some analyses of galaxy clustering rely on partitioning a sample into subsamples based on their observed properties (Skibba et al. 2006; Croft 2013; Alam et al. 2017). The effects we model in this paper are likely to be relatively more important for these analyses, as they will have different strengths for sub-samples with different galaxy properties.

4 SPECIAL CASE: SDSS III CMASS SAMPLE

The SDSS III CMASS sample is one of the key target datasets where we have a large number of massive galaxies with photometric and spectroscopic observations. We use this sample as an example, computing the effects of relativistic beaming and Doppler shifting in detail. This analysis can be easily extended to other surveys. We first briefly describe the sample and introduce the relevant quantity necessary to understand the CMASS target selection.

4.1 CMASS Sample

We use data included in data release 12 (DR12; Reid et al. 2016; Alam et al. 2015) of the Sloan Digital Sky Survey (SDSS; York et al. 2000). SDSS I, II (Abazajian et al. 2009) and III (Eisenstein et al. 2011) used a drift-scanning mosaic CCD camera (Gunn et al.

1998) to image 14555 square degrees of the sky in five photometric bands (Fukugita et al. 1996; Smith et al. 2002; Doi et al. 2010) to a limiting magnitude of $r < 22.5$ using the 2.5-m Sloan Telescope (Gunn et al. 2006) at the Apache Point Observatory in New Mexico. The imaging data were processed through a series of SDSS pipelines (Lupton et al. 1999; Pier et al. 2003; Padmanabhan et al. 2008). Aihara et al. (2011) reprocessed all of the SDSS imaging data in Data Release 8 (DR8). The Baryon Oscillation Spectroscopic survey (BOSS; Dawson et al. 2013) was designed to obtain spectra and redshifts for 1.35 million galaxies covering 10,000 square degrees of sky. These galaxies were selected from the SDSS DR8 imaging. (Blanton et al. 2003a) developed a tiling algorithm that is adaptive to the density of targets on the sky and this was used for targeting in BOSS. BOSS used double-armed spectrographs Smee et al. (2013) to obtain the spectra. BOSS resulted in a homogeneous data set with a high redshift completeness of more than 97% over the full survey footprint. The redshift extraction algorithm used in BOSS is described in Bolton et al. (2012). Eisenstein et al. (2011) provides a summary and Dawson et al. (2013) provides a detailed description of the survey design.

We use the CMASS sample of galaxies (Bolton et al. 2012) from data release 12 (Alam et al. 2015). The CMASS sample contains 7,65,433 Luminous Red Galaxies (LRGs) covering 9376 square degrees in the redshift range $0.44 < z < 0.70$, which correspond to an effective volume of 10.8 Gpc^3 . We used co-added spectra for each galaxy in our analysis⁴.

4.1.1 CMASS Target Selection

The photometrically identified objects in the SDSS imaging catalog (Data Release 8:DR8⁵) are used as the parent sample for selecting the galaxies to be targeted for spectroscopic observations. The parent catalog covered 7606 deg^2 in the Northern Galactic Cap (NGC) and 3172 deg^2 in the Southern Galactic Cap (SGC). The photometric sample contains flux observed in five photometric bands (u, g, r, i, z). The target selection for the CMASS sample uses two types of magnitude provided by the SDSS imaging pipeline. The imaging pipeline fits exponential and deVaucouleurs profiles for each of the five photometric band to provide the fluxes $f_{\text{exp}}^{\text{band}}$ and $f_{\text{dev}}^{\text{band}}$ respectively. These fluxes are used to define two different kinds of flux, named ‘‘model’’ and ‘‘cmodel’’ and given by the following equations.

$$f_{\text{mod,cmod}}^{\text{band}} = (1 - P_{\text{mod,cmod}})f_{\text{exp}}^{\text{band}} + P_{\text{mod,cmod}}f_{\text{dev}}^{\text{band}}. \quad (10)$$

Here P_{mod} is a real number between 0 and 1, and P_{cmod} is an integer which can be either 0 or 1. The imaging pipeline fits the observed flux to obtain values of $P_{\text{mod,cmod}}$. The main difference between model and cmodel flux is that the model flux results from the use of a linear combination of exponential and deVaucouleurs profiles, whereas the cmodel flux uses the best-fitting profile. The model and cmodel fluxes are converted to magnitudes as follows:

$$\text{mag}_{\text{band}} = 22.5 - 2.5 \log(f^{\text{band}}) - C_{\text{extinction}}, \quad (11)$$

⁴ The co-added version of the spectrum used in our analysis can be downloaded from http://data.sdss3.org/sas/dr12/boos/spectro/redux/v5_7_0/spectra/lite/. The basic description of the SDSS optical spectra can be found over http://www.sdss.org/dr12/spectro/spectro_basics

⁵ <http://www.sdss3.org/dr8>

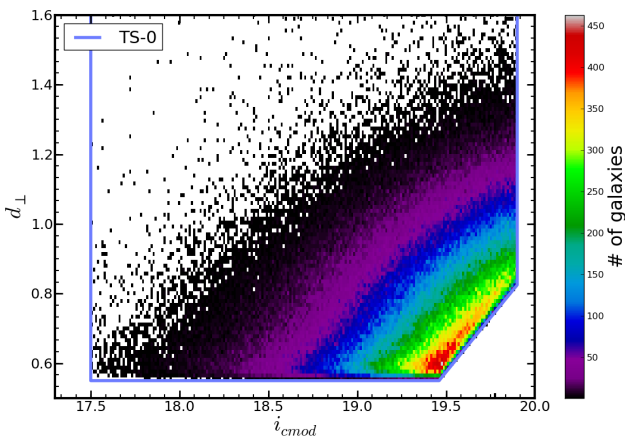


Figure 2. The density of galaxies in the CMASS sample in colour-magnitude space. The parameter d_{perp} is defined in Equation 15. The red colour indicates a high density and black shows low density. The solid blue line represents the CMASS target selection criteria.

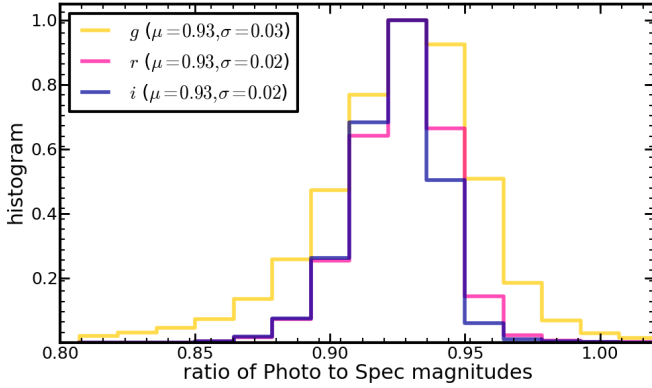


Figure 3. The histogram of the ratio of magnitudes from spectra to the photometric magnitude for g , r and i bands. The mean of the ratio is 0.93 which indicates that the magnitudes measured from spectra are larger (flux from spectra is smaller). This is because the fibres cover only $2''$ which is smaller than the mean size of a galaxy in the sample. This plot also shows that the scatter in this ratio of the two magnitudes is quite small.

where fluxes are in nanomaggies and mag_{band} can be any of the five photometric bands u, g, r, i, z . The $C_{\text{extinction}}$ is the galactic extinction correction for the galaxy using the dust maps of [Schlegel et al. \(1998\)](#). The main criteria used in CMASS target selection are as follows:

$$17.5 < i_{\text{cmod}} < 19.9 \quad (12)$$

$$d_{\perp} > 0.55 \quad (13)$$

$$i_{\text{cmod}} < 1.6(d_{\perp} - 0.8) + 19.86 \quad (14)$$

The CMASS targets are selected to create a constant stellar mass sample. A galaxy evolution model incorporating the redshift evolution of band magnitudes is used to determine the magnitude cuts that lead to the required sample. Hence the selection (using model magnitudes as cuts) is applied without any K-correction. There are several other criteria used for the target selection but they affect a very small number of objects and are not relevant for our study. The full list of target selection rules is provided in [Reid et al. \(2016\)](#). The quantity i_{cmod} is the cmodel magnitude for photometric band i . The quantity d_{\perp} is a linear combination of the colour $g - r$ and $r - i$ based on model magnitude as follows:

$$d_{\perp} = (r_{\text{mod}} - i_{\text{mod}}) - \frac{1}{8}(g_{\text{mod}} - r_{\text{mod}}), \quad (15)$$

where $g_{\text{mod}}, r_{\text{mod}}, i_{\text{mod}}$ are the model magnitudes for the photometric bands g, r and i respectively. The Figure 2 shows the distribution of galaxies in the final CMASS sample (DR12) in the $i_{\text{cmod}} - d_{\perp}$ plane. The solid line shows the target selection rule as stated in equation 12, 13 and 14.

4.2 Spectro-Photometry

We use SDSS observed SEDs as a template to study the relativistic effects. We assume the observed SEDs are good representation of the galaxy population and treated them as if they were emitted SED of galaxies. We transform each of the observed spectra according to equation 9 for a given β and θ . We then obtain the flux in differ-

ent photometric bands by integrating the spectra with the response function for each band:

$$f_{\text{spec}}^{\text{band}} = \int d\lambda f(\lambda) R^{\text{band}}(\lambda) C^{\text{band}}, \quad (16)$$

where $f(\lambda), R(\lambda)$ represents the flux and photometric band response for wavelength λ . The parameter C^{band} is the calibration factor which is obtained using the fibre flux of 10,000 galaxies. The calibration factors obtained for g, r and i bands are $((2.3, 3.3, 6.1)^{-3})$ respectively. The fibre flux is another flux provided in the SDSS imaging catalog. It represents the flux obtained in the photometric survey with the aperture of spectroscopic fibre for each band ⁶. The aperture of $2''$ in diameter is assumed for calculating fibre flux, which is appropriate for the BOSS spectrograph. The spectroscopic flux is converted to magnitude using equation 11. The spectroscopic magnitude is typically smaller than the corresponding photometric magnitude because fibres cover only the central part of galaxies. We have found that the spectroscopic magnitudes can be converted to photometric magnitudes using a simple multiplication factor of 0.93. The Figure 3 shows the histogram of the ratio of model magnitude to the spectroscopic magnitude. For each of g, r and i band the ratio of magnitudes has mean at 0.93 with a scatter of 0.03 for g band and 0.02 for both r and i band. We therefore obtain the cmodel magnitude from the spectroscopic magnitude using a multiplication factor of 0.93 ($i_{\text{cmod}}^{\text{spec}} = 0.93i^{\text{spec}}$).

4.3 Magnitude and colour evolution

The local gravitational interactions of galaxies causes them to have peculiar velocities. These peculiar velocities cause the observed SEDs of galaxies to be different from the true SEDs. This can change the observed magnitude and colour of galaxies. We systematically investigate these changes for grid of peculiar velocity magnitudes and directions from the line-of-sight. We transform the observed spectra of each galaxy using β values between -0.01 and 0.01 and θ between 0° and 90° . We find that adding relativistic effects to spectra shifts the galaxies in the target selection plane. Not suprisingly, these shifts in colour are sensitive to the galaxy spectra themselves and therefore depend on the stellar mass and redshift of galaxies. The Figure 4 shows the tracks of galaxies in the target selection colour-magnitude plane. Each line with an arrowhead shows the path followed by the galaxies in the sample as peculiar velocity is varied. The tail of the line corresponds to the colour-magnitude of the galaxy when it is moving away from the observer with $\beta = -0.01$ (speed of 3000 km s^{-1}) and the arrowhead correspond to the case when it is moving towards the observer with the same speed (i.e. we are showing the difference in assigning β from -0.01 (tail) to $+0.01$ (head)). The colour of the track indicates the redshift of the galaxy. Note that in the plot we only show a very small illustrative sub-sample of the full CMASS dataset, and we restrict ourselves to velocity directions directly aligned with the line-of-sight. The black thick solid line shows the CMASS target selection as described in equations 12, 13 and 14. We also show 3 more restrictive target selection criteria using other solid lines. The target selection criterion TS-n is given by the following equation:

⁶ <http://www.sdss.org/dr12/algorithms/magnitudes/>

$$17.5 < i_{\text{cmod}} < 19.9 - 0.05n \quad (17)$$

$$d_{\perp} > 0.55 + 0.03n \quad (18)$$

$$i_{\text{cmod}} < 1.6(d_{\perp} - 0.8 - 0.05n) + 19.86, \quad (19)$$

where n is either 0,1,2, or 3, which represent different target selections TS-0,TS-1,TS-2 and TS-3 respectively. TS-0 is the actual CMASS target selection. Notice that these additional target selections are defined such that the shape of the target selection region in this plane remains unchanged. The tracks of galaxies show that the magnitudes (plotted on the x-axis) decrease (becomes brighter) when galaxies move towards the observer and increase (becomes dimmer) when they moves away as per our expectation. This leads to galaxies at higher redshifts which are close to the magnitude limit of the target selection being moved inside the sample when their velocity is towards the observer and being moved outside while their velocity is away. The colour cuts can however reverse this trend as shown by the galaxies close to the lower limit of d_{\perp} , which are at lower redshifts. These galaxies move inside the sample when they have velocities away from the observer and moves outside the sample with velocities towards the observer. It should be also noted that the effects shown in this plot are exaggerated by roughly an order of magnitude compared to the typical case for galaxies, as we are showing results for galaxy velocities as high as 3000 km s^{-1} .

4.4 Impact on Final Obtained Sample

Because the peculiar velocities of galaxies vary spatially, the relativistic effects will spatially modulate the observed SEDs of galaxies, which will in turn affect the observed magnitudes and colours. Therefore, a fraction of galaxies with colours and magnitudes originally within our target selection will move out of the sample and also some galaxies from outside the sample will move into it. This affects the observed number density of galaxies in the final sample. The modulations introduced in the observed number density will also be correlated with several other properties of galaxies for example stellar mass, redshift and velocity. In order to quantify these effects, we bin our sample in redshift and stellar mass. We create 10 bins in redshift between 0.4 and 0.8 and 10 bins in logarithm of stellar mass between $10^{10.8} M_{\odot}$ and $10^{13} M_{\odot}$. Naively one might think that the sample doesn't contain information on galaxies lost due to such effects and it should be impossible to correct for these lost galaxies. However, this is not the case if we work under the assumption that the lost (and extra) galaxies are part of the same distribution, and that galaxies properties and dynamics are smoothly varying. As long as we are not dominated by noise where we overfit small fluctuations in small bins of properties our results should be independent of binning used in the sample. For each stellar mass and redshift bin, we compute the initial number of galaxies (N_{TS}^i) in the sample. We then transform the galaxies as if they were moving with velocity $v = \beta c$ along a direction at angle θ from the line-of-sight. We then reapply the target selection boundaries to count the final number of galaxies in the sample (N_{TS}^f). The relativistic effects due to peculiar motion of galaxies imply that the number of galaxies in the observed sample will be multiplied by the fraction $N_{\text{TS}}^f/N_{\text{TS}}^i$. Therefore, in clustering analysis if we would like to compensate for the number density modulation due to relativistic effects we should weight each galaxy by w_{rel} , where

$$w_{\text{rel}} = N_{\text{TS}}^i/N_{\text{TS}}^f \quad (20)$$

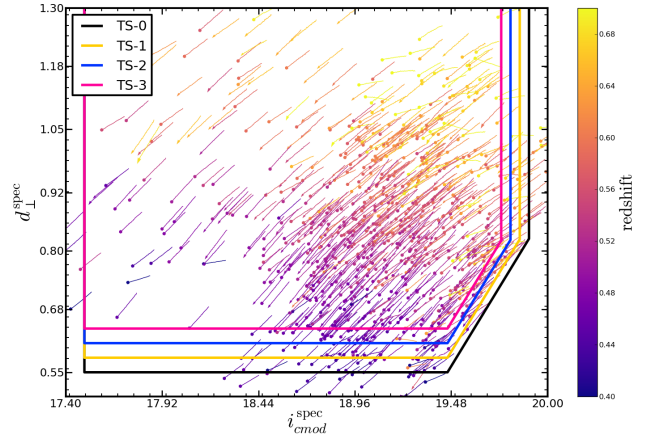


Figure 4. The effects of galaxy motion on observed galaxy colour and magnitude. The solid thick lines of different colours show the different versions of our target selection criteria. The black solid line shows the CMASS original target selection. Other solid lines shows the variant of CMASS target selection described in equation 19. Each line with an arrow head shows how an individual galaxy will move in this space as we assign it a different velocity. The arrow-head shows the observed colour-magnitude when galaxies are moving towards the observer with a speed of 3000 km s^{-1} and the tail point shows the colour-magnitude when it moves with speed of 3000 km s^{-1} away from the observer. The colour of the arrow itself indicates the redshift of the galaxy. Note that at small redshift a galaxy moving towards observer will cross the colour cut to move out of the sample whereas at higher redshift the galaxy moving towards us will become brighter and cross the lower magnitude cut to move inside the sample. Note that we only show a very small illustrative sub-sample of the full CMASS dataset, and we restrict ourselves to velocity directions directly aligned with the line-of-sight. It should be also noted that the effects shown in this plot are exaggerated by roughly an order of magnitude compared to the typical case for galaxies, as we are showing results for galaxy velocities as high as 3000 km s^{-1} .

We have obtained the w_{rel} for each bin as a function of β and θ of the galaxy. Figure 5 shows the weights obtained for some of the redshift and stellar mass bins as the function of β and θ . The different colours correspond to different redshift bins, while the different line styles correspond to different stellar mass bins. The left panel shows w_{rel} with β between -0.01 and 0.01 and $\theta = 0$. The value $\beta = -0.01$ corresponds to galaxies moving with a speed 3000 km s^{-1} away from the observer and $\beta = 0.01$ galaxies moving at 3000 km s^{-1} towards the observer. At higher redshifts the galaxies moving towards the observer (positive β) have weight smaller than 1. They will appear brighter and hence will be seen in larger number than if they were at rest with respect to the observer. The weight in this case is therefore smaller than unity, to compensate for the higher number of observed galaxies. The weights vary with stellar mass, galaxies with higher stellar mass having larger weights.

These trends change for lower redshifts however. Below approximately $z = 0.5$, galaxies moving towards the observer have weights larger than 1. This is due the fact that the galaxies at lower redshift are less likely to be close to the magnitude limit of the sample than they are to the colour cut. When they move towards the observer they cross through the colour cut and out of the sample. This causes a reverse trend with β which is different to that at higher redshifts. This can be seen in Figure 4 by following the tracks of these galaxies as β is varied. The middle and right panels of Figure 5 shows the dependence of w_{rel} on the direction of galaxy

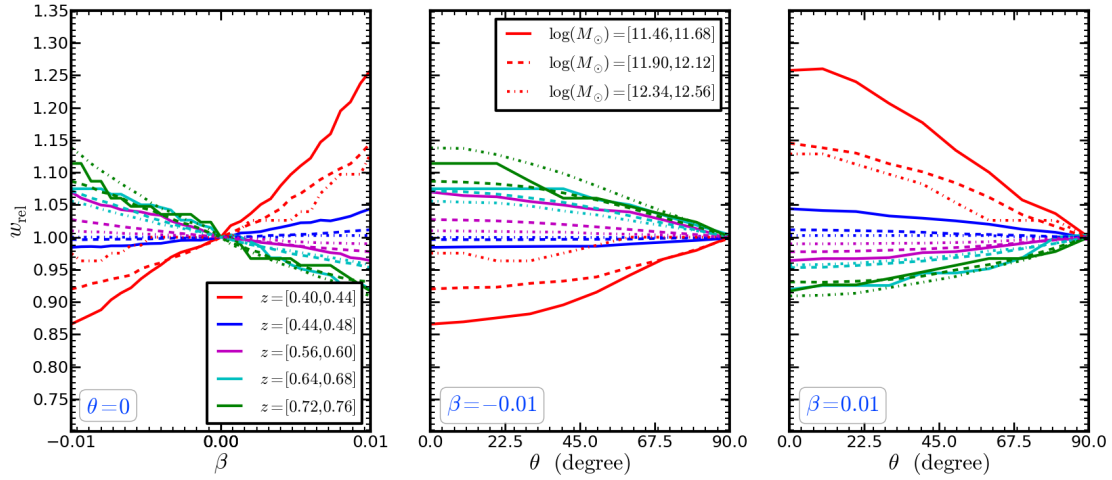


Figure 5. The relativistic weights for a galaxy given its redshift, stellar mass and velocity vector. The different colours indicate different redshift bins and different line-styles indicate different stellar mass bins. The left panel shows the w_{rel} with velocity of the galaxy in units of the speed of light along line-of-sight. The central and right panel shows the weight dependence on the direction of velocity from line-of-sight for $\beta = -0.01$ ($v=3000 \text{ km s}^{-1}$ away from observer) and $\beta = 0.01$ ($v=3000 \text{ km s}^{-1}$ towards the observer) respectively.

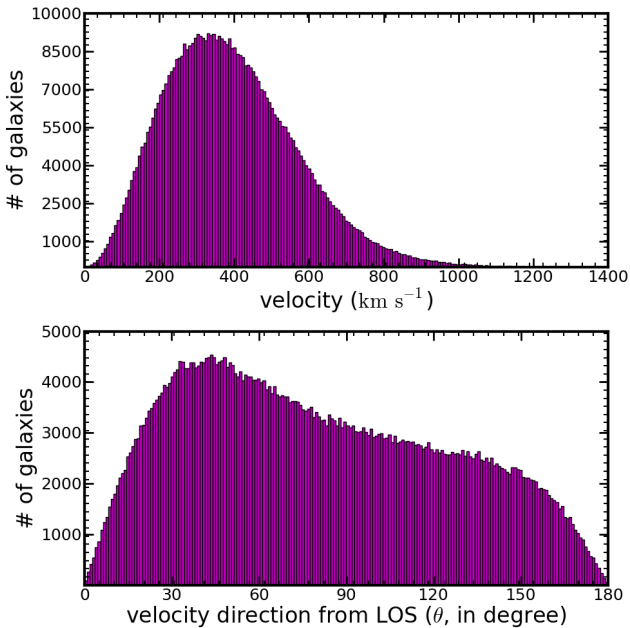


Figure 6. Estimated galaxy peculiar velocities in the SDSS III CMASS galaxy redshift sample. The velocity vectors for each galaxy were estimated using a perturbation theory based reconstruction algorithm. The top panel shows the distribution of the magnitudes of galaxy velocities in the sample. The bottom panel shows the distribution of velocity directions, where $\theta = 0^\circ$ indicates that a galaxy is moving along line of sight away from observer and $\theta = 180^\circ$ that the galaxy is moving directly towards the observer.

velocity θ for velocities with positive and negative β . These results show the importance of considering the full velocity vector rather than just the line-of-sight component.

4.5 Predicting the galaxy peculiar velocities

In order to associate relativistic weights to each individual galaxy, the galaxy velocity is required. We estimate the velocity for each galaxy in the sample using a reconstruction approach. We use a publicly available reconstruction code⁷ which estimates the velocities of galaxy in our sample using perturbation theory (White 2015a,b). The reconstruction code first computes the number density (ρ) of galaxies on a grid using a cloud-in-cell assignment scheme. The number density is then converted to density contrast (δ) which is divided by a large scale bias b to yield the mass fluctuation in the cell. We use the value $b = 2.1$ measured in our analysis Alam et al. (see companion paper: 2017). This mass fluctuation is then smoothed using a Gaussian kernel of width R_f (the smoothing scale). Our chosen value of $R_f = 10 \text{ h}^{-1} \text{ Mpc}$ is motivated by the results of (Vargas-Magaña et al. 2015). The reconstruction code then solves for the displacement field (Zel'dovich 1970) and provides the displaced position for each galaxy (White 2015a). We use the displaced position to obtain the peculiar velocities of galaxies using following equation:

$$\vec{v} = afH(\vec{r}_{\text{obs}} - \vec{r}_{\text{recon}}), \quad (21)$$

where $H = 100 \text{ (h}^{-1} \text{ Mpc)/km s}^{-1}$, $a = 1/(1+z)$ is the scale factor. We approximate the linear growth rate of perturbations $f = d \ln D / d \ln a$ as $f = \Omega_m(z)^{0.55}$. Figure 6 shows the distribution of galaxy velocities obtained using this procedure. In the top panel it can be seen that most of the galaxies have velocities between $200 - 600 \text{ km s}^{-1}$. The bottom panel shows the distribution of the angles between the velocities in the line of sight. The detailed shape of this distribution depends on the geometry the survey.

In an isotropic universe we would expect the velocity distribution to be isotropic. This in spherical polar coordinates would yield a sin function for the velocity distribution with angle. Since the

⁷ github repo: https://github.com/martinjameswhite/recon_code/

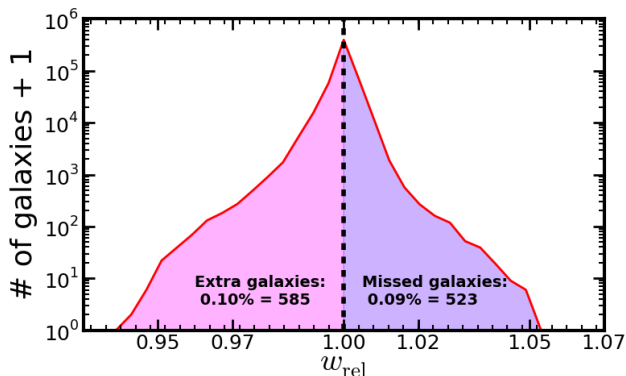


Figure 7. The distribution of the relativistic weights w_{rel} for the CMASS galaxy redshift sample. The x-axis is w_{rel} and the y-axis displays the binned number of galaxies on logarithmic scale. The galaxies with $w_{\text{rel}} < 1$ have higher probability of being in the sample. We estimate that 0.16% more such galaxies have been added to the sample because of their peculiar velocities. Galaxies with weights $w_{\text{rel}} > 1$ have a lower probability of being in the sample. From these we calculate that 0.11% of the sample which would be have been within the colour-magnitude cuts is excluded because of the effect of peculiar velocities.

survey geometry is a cone we are sub-sampling a cone to estimate the velocity distribution. Simply sub-sampling any part of universe with any geometric shape shouldn't change the velocity distribution either. However, we are estimating the velocity using the sub-sampled galaxy distribution. While solving the Poisson equation the effect of missing galaxies will alter the estimated velocities. In the simplest picture, since we sample a cone, this implies an area increasing as we move farther from the observer, and so more galaxies should be moving away from the observer than towards the observer. We believe this to be the reason for the sloping distribution between 30 and 150 degree in the lower panel of Figure 6. The angle zero degrees is that pointing away from observer and 180 degrees denotes pointing towards the observer in our convention.

We note that these velocities are predicted using perturbation theory which is not accurate on small scales where non-linear clustering occurs. On scales below our smoothing scale, a number of galaxies will be moving significantly faster than the predicted velocity. This will be particularly true in virialised objects such as galaxy clusters. Our estimate of the strength of relativistic effects will therefore tend to be an underestimate. We also note that the fact that the velocities are predicted using already modulated field will introduce a second order relativistic correction which we expect to be much smaller and leave for future studies.

4.6 Impact on Clustering

We now examine how relativistic sample selection effects alter the results of standard clustering analyses of the CMASS galaxy redshift sample. We use the observational data for the CMASS sample to compute the weights w_{rel} which compensate each galaxy for the effect of Doppler shifting and beaming (see section 4.4). These weights are a function of the redshift, stellar mass and velocity vector of the galaxy. The relativistic correction therefore involves applying the weights before computing the two-point clustering of the galaxy sample. The galaxy catalog contains the redshift and stellar mass of each of the galaxy. We estimate the velocity vector of the

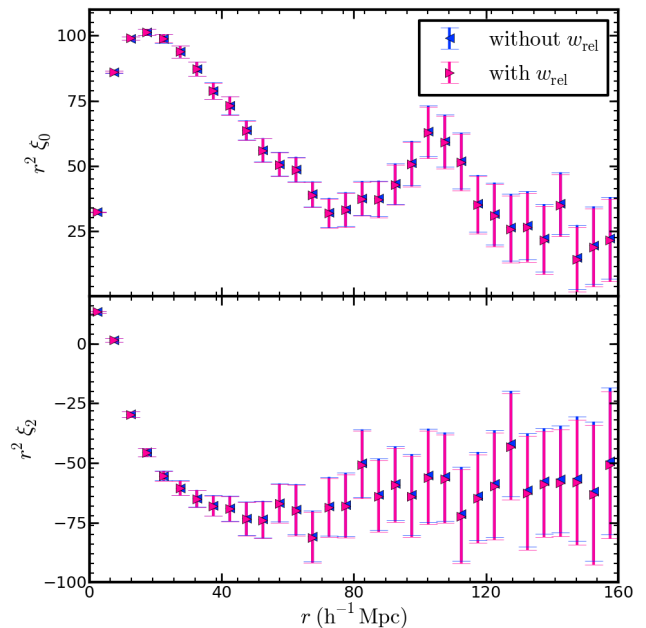


Figure 8. The two point galaxy auto-correlation function with and without the effect of relativistic weights. The top panel shows the monopole and the bottom panel shows the quadrupole moment of the correlation function. The blue points represents the measurement without relativistic weight and the magenta points are with the relativistic weight correction.

galaxy using the perturbation theory approach described in section 4.5. Figure 7 shows the distribution of w_{rel} in the CMASS sample. We can see that the distribution of weights is not symmetric due to the fact that the luminosity function is non-uniform and hence there are more galaxies which scatters into the sample compared to those that scatters out of the sample. We estimate that around 0.10% (~ 585 galaxies) of the CMASS sample should not have been targeted and around 0.09% (~ 523 galaxies) should have been in the sample, but were not observed.

We have computed the two-point clustering of CMASS with and without the relativistic weights. We use the Landy-szalay (Landy & Szalay 1993) estimator, and the results are shown in Figure 8. The top panel shows the monopole of the correlation function and the bottom panel the quadrupole moment. The error bars on the clustering were computed by dividing the entire sample into 61 jackknife regions, see Alam et al. (2017) for more details. We find that the effects of these weights are much smaller than the statistical errors on the clustering measurement.

We therefore do not expect that any of the standard large scale structure analyses (such as BAO measurement or redshift space distortions) will show significant effects in current surveys. We should bear in mind though, that as the samples get larger and probe fainter magnitudes these effects might start to become more important for future surveys.

5 CONCLUSION

We have used the SDSS III BOSS CMASS galaxy sample to examine the impact of relativistic effects on observed galaxy SEDs. We have discussed how the effects on SEDs will translate to observed fluxes and hence will impact the target selection of galaxy redshift

surveys. We have found that galaxies can move both in and out of the sample depending on their peculiar motion. We have investigated these effects for the CMASS target selection as a function of redshift, stellar mass, magnitude and direction of galaxy velocity. In order to estimate the effect on clustering statistics, we have also used perturbation theory to predict the galaxy velocities from the galaxy density field. These velocities provide the information we need to gauge the impact of relativistic effects on individual galaxies.

We have computed weights that can be used to cancel out the relativistic effects on target selection. We studied the galaxy two-point correlation function with and without these weights, finding an impact on the clustering signal which is much smaller than the current statistical errors. This should not therefore affect current large scale structure analyses such as baryon acoustic oscillation measurement or estimates of the growth rate from redshift space distortions. We expect that these effects will be more significant when one is looking at galaxy clustering weighted by one of the properties which are affected by relativistic effects such as luminosity, photometric magnitude etc. We also expect these effects to be more significant when surveys are deeper and hence future surveys should be analyzed with such effects in mind.

One of the main motivations to study these effects is to understand how relativistic beaming and doppler shift modulate the density field and change galaxy clustering. If clustering statistics are chosen carefully and galaxy samples are large enough, then these effects can in principle be detected. (Kaiser 2013) has shown that these effects can contribute to the asymmetry in galaxy clustering around clusters which is used to infer the gravitational redshift profile (e.g., Cappi 1995; Kim & Croft 2004; Wojtak et al. 2011; Zhao et al. 2013; Sadeh et al. 2015). Relativistic effects on large-scale clustering have also been computed using perturbation theory in full General Relativity (e.g., McDonald 2009; Yoo et al. 2012; Bonvin et al. 2014). The results in our paper have motivated the form of the beaming effect included in a companion paper Zhu et al. (2017). We have applied them to N-body simulations in order to estimate the line-of-sight asymmetry in the non-linear scale cross-correlation function of two galaxy populations with different halo masses. The models are also used in our other companion paper Alam et al. (2017), which provides the first measurement of line-of-sight asymmetry in the CMASS sample.

ACKNOWLEDGMENTS

This work was supported by NSF grant AST1412966. SA is also supported by the European Research Council through the COSFORM Research Grant (#670193). SA and SH are supported by NASA grants 12-EUCLID11-0004 during part of this study. We would like to thank Ayesha Fatima for going through the early draft and helping us making the text much more clear.

SDSS-III is managed by the Astrophysical Research Consortium for the Participating Institutions of the SDSS-III Collaboration including the University of Arizona, the Brazilian Participation Group, Brookhaven National Laboratory, Carnegie Mellon University, University of Florida, the French Participation Group, the German Participation Group, Harvard University, the Instituto de Astrofísica de Canarias, the Michigan State/Notre Dame/JINA Participation Group, Johns Hopkins University, Lawrence Berkeley National Laboratory, Max Planck Institute for Astrophysics, Max Planck Institute for Extraterrestrial Physics, New Mexico State University, New York University, Ohio State University, Pennsyl-

vania State University, University of Portsmouth, Princeton University, the Spanish Participation Group, University of Tokyo, University of Utah, Vanderbilt University, University of Virginia, University of Washington, and Yale University.

REFERENCES

- Abazajian K. N., et al., 2009, *ApJS*, **182**, 543
- Abe F., et al., 1997, in Ferlet R., Maillard J.-P., Raban B., eds, *Variables Stars and the Astrophysical Returns of the Microlensing Surveys*. p. 75
- Aihara H., et al., 2011, *ApJS*, **193**, 29
- Alam S., et al., 2015, *ApJS*, **219**, 12
- Alam S., Zhu H., Croft R. A. C., Ho S., E. G., 2017, *MNRAS*, pp xx–xx
- Arnaud M., et al., 1994, *Experimental Astronomy*, **4**, 265
- Bacon D. J., Andrianomena S., Clarkson C., Bolejko K., Maartens R., 2014, *MNRAS*, **443**, 1900
- Bardeen J. M., Bond J. R., Kaiser N., Szalay A. S., 1986, *ApJ*, **304**, 15
- Bassett B., Hlozek R., 2010, *Baryon acoustic oscillations*. p. 246
- Bauer F., de Kat J., 1998, in Beletic J., Amico P., eds, *Astrophysics and Space Science Library Vol. 228, Optical Detectors for Astronomy*. p. 191, doi:10.1007/978-94-011-5262-4_29
- Beletic J., Amico P., eds, 1998, *Optical detectors for astronomy Astrophysics and Space Science Library Vol. 228*, doi:10.1007/978-94-011-5262-4.
- Bernardeau F., Colombi S., Gaztañaga E., Scoccimarro R., 2002, *Phys. Rep.*, **367**, 1
- Blake C., et al., 2011, *MNRAS*, **418**, 1707
- Blanton M. R., Lin H., Lupton R. H., Maley F. M., Young N., Zehavi I., Loveday J., 2003a, *AJ*, **125**, 2276
- Blanton M. R., et al., 2003b, *AJ*, **125**, 2348
- Bock J., SPHEREx Science Team 2016, in *American Astronomical Society Meeting Abstracts*. p. 147.01
- Bolton A. S., et al., 2012, *AJ*, **144**, 144
- Bonvin C., 2014, *Classical and Quantum Gravity*, **31**, 234002
- Bonvin C., Hui L., Gaztañaga E., 2014, *Phys. Rev. D*, **89**, 083535
- Boulade O., 1998, in Beletic J., Amico P., eds, *Astrophysics and Space Science Library Vol. 228, Optical Detectors for Astronomy*. p. 203, doi:10.1007/978-94-011-5262-4_30
- Bruni M., Lyth D. H., 1994, *Physics Letters B*, **323**, 118
- Cappi A., 1995, *A&A*, **301**, 6
- Coil A. L., 2013, *The Large-Scale Structure of the Universe*. p. 387, doi:10.1007/978-94-007-5609-0_8
- Cole S., Kaiser N., 1989, *MNRAS*, **237**, 1127
- Colless M., et al., 2003, preprint, (arXiv:astro-ph/0306581)
- Comer G. L., Deruelle N., Langlois D., Parry J., 1994, *Phys. Rev. D*, **49**, 2759
- Content R., Sharples R. M., Blake S., Talbot R. G., 2010, in *Space Telescopes and Instrumentation 2010: Optical, Infrared, and Millimeter Wave*. p. 77312Y, doi:10.1117/12.857937
- Croft R. A. C., 2013, *MNRAS*, **434**, 3008
- DESI Collaboration et al., 2016, preprint, (arXiv:1611.00036)
- Dawson K. S., et al., 2013, *AJ*, **145**, 10
- Doi M., et al., 2010, *AJ*, **139**, 1628
- Durrer R., 1994, *Fundamentals Cosmic Phys.*, **15**, 209
- Einstein A., 1916, *Annalen Der Physik*, **49**, 770
- Eisenstein D. J., et al., 2005, *ApJ*, **633**, 560
- Eisenstein D. J., et al., 2011, *AJ*, **142**, 72
- Fukugita M., Ichikawa T., Gunn J. E., Doi M., Shimasaku K., Schneider D. P., 1996, *AJ*, **111**, 1748
- Garilli B., et al., 2014, *A&A*, **562**, A23
- Geller M. J., Huchra J. P., 1989, *Science*, **246**, 897
- Gilbank D. G., Gladders M. D., Yee H. K. C., Hsieh B. C., 2011, *AJ*, **141**, 94
- Gladders M. D., Yee H. K. C., 2005, *ApJS*, **157**, 1
- Goodman J., 2013, <http://www.astro.princeton.edu/~jeremy/heap.pdf>

- Gunn J. E., et al., 1998, *AJ*, **116**, 3040
- Gunn J. E., et al., 2006, *AJ*, **131**, 2332
- Hill G. J., et al., 2008, in Kodama T., Yamada T., Aoki K., eds, *Astronomical Society of the Pacific Conference Series Vol. 399, Panoramic Views of Galaxy Formation and Evolution*. p. 115 ([arXiv:0806.0183](https://arxiv.org/abs/0806.0183))
- Hogg D., 1997, <http://cosmo.nyu.edu/hogg/sr/sr.pdf>
- Hogg D. W., Baldry I. K., Blanton M. R., Eisenstein D. J., 2002, *ArXiv Astrophysics e-prints*,
- Jones D. H., et al., 2009, *MNRAS*, **399**, 683
- Kaiser N., 2013, *MNRAS*, **435**, 1278
- Kaiser N., Hudson M. J., 2015, *MNRAS*, **450**, 883
- Kaiser N., et al., 2010, in *Ground-based and Airborne Telescopes III*. p. 77330E, [doi:10.1117/12.859188](https://doi.org/10.1117/12.859188)
- Kim Y.-R., Croft R. A. C., 2004, *ApJ*, **607**, 164
- Kopeikin S. M., Ramirez J., Mashhoon B., Sazhin M. V., 2001, *Physics Letters A*, **292**, 173
- Lagos M., Baker T., Ferreira P. G., Noller J., 2016, preprint, ([arXiv:1604.01396](https://arxiv.org/abs/1604.01396))
- Landy S. D., Szalay A. S., 1993, *ApJ*, **412**, 64
- Liddle A. R., Lyth D. H., 1993, *Phys. Rep.*, **231**, 1
- Liske J., et al., 2015, *MNRAS*, **452**, 2087
- Lupton R. H., Gunn J. E., Szalay A. S., 1999, *AJ*, **118**, 1406
- Ma C.-P., Bertschinger E., 1994, *ArXiv Astrophysics e-prints*,
- McDonald P., 2009, *J. Cosmology Astropart. Phys.*, **11**, 026
- Ménard B., Scranton R., Fukugita M., Richards G., 2010, *MNRAS*, **405**, 1025
- Momcheva I. G., et al., 2015, preprint, ([arXiv:1510.02106](https://arxiv.org/abs/1510.02106))
- Mukhanov V. F., Feldman H. A., Brandenberger R. H., 1992, *Phys. Rep.*, **215**, 203
- Newman J. A., et al., 2013, *ApJS*, **208**, 5
- Padmanabhan N., et al., 2008, *ApJ*, **674**, 1217
- Peebles P. J. E., Yu J. T., 1970, *ApJ*, **162**, 815
- Pier J. R., Munn J. A., Hindsley R. B., Hennessy G. S., Kent S. M., Lupton R. H., Ivezić Ž., 2003, *AJ*, **125**, 1559
- Prakash A., et al., 2016, *ApJS*, **224**, 34
- Reid B., et al., 2016, *MNRAS*, **455**, 1553
- Sadeh I., Feng L. L., Lahav O., 2015, *Physical Review Letters*, **114**, 071103
- Schlegel D. J., Finkbeiner D. P., Davis M., 1998, *ApJ*, **500**, 525
- Schmidt F., Leauthaud A., Massey R., Rhodes J., George M. R., Koekemoer A. M., Finoguenov A., Tanaka M., 2012, *ApJ*, **744**, L22
- Schuecker P., 1996, *MNRAS*, **279**, 1057
- Shectman S. A., Landy S. D., Oemler A., Tucker D. L., Lin H., Kirshner R. P., Schechter P. L., 1996, *ApJ*, **470**, 172
- Skibba R., Sheth R. K., Connolly A. J., Scranton R., 2006, *MNRAS*, **369**, 68
- Smee S. A., et al., 2013, *AJ*, **146**, 32
- Smith J. A., Tucker D. L., Allam S. S., Jorgensen A. M., 2002, in *American Astronomical Society Meeting Abstracts*. p. #104.08
- Spergel D., et al., 2013, preprint, ([arXiv:1305.5425](https://arxiv.org/abs/1305.5425))
- Strauss M. A., et al., 2002, *AJ*, **124**, 1810
- Takada M., 2010, in Kawai N., Nagataki S., eds, *American Institute of Physics Conference Series Vol. 1279, American Institute of Physics Conference Series*. pp 120–127, [doi:10.1063/1.3509247](https://doi.org/10.1063/1.3509247)
- Teerikorpi P., 1997, *ARA&A*, **35**, 101
- Vargas-Magaña M., Ho S., Fromenteau S., Cuesta A. J., 2015, preprint, ([arXiv:1509.06384](https://arxiv.org/abs/1509.06384))
- White M., 2015a, *ZeldovichRecon: Halo correlation function using the Zeldovich approximation*, *Astrophysics Source Code Library* ([ascl:1512.016](https://ascl.net/1512.016))
- White M., 2015b, *MNRAS*, **450**, 3822
- Wojtak R., Hansen S. H., Hjorth J., 2011, *Nature*, **477**, 567
- Yoo J., 2014, *Classical and Quantum Gravity*, **31**, 234001
- Yoo J., Hamaus N., Seljak U., Zalduendo M., 2012, *Phys. Rev. D*, **86**, 063514
- York D. G., et al., 2000, *AJ*, **120**, 1579
- Zel'dovich Y. B., 1970, *A&A*, **5**, 84
- Zhao H., Peacock J. A., Li B., 2013, *Phys. Rev. D*, **88**, 043013
- Zhu H., Alam S., Croft R. A. C., Ho S., E. G., 2017, *xxx*, pp xx–xx